

Simulation of the liquid pool for VT3-1 titanium alloy during vacuum arc remelting process.

E.N. Kondrashov[†], M.I. Musatov[‡], A.Yu. Maximov[†],
A.E. Goncharov[†], and L.V. Konovalov[†]

[†] JSC VSMPO-AVISMA Corporation, Parkovaya str. 1, Verkhnyaya Salda, 624760, Sverdlovsk region, Russian Federation.

[‡] JSC VILS, Gorbunova str. 2, Moscow, 121596, Russian Federation.

E-mail: evgeniy.kondrashov@vsm-po.ru

Abstract.

This article describes a simple heat model of the vacuum arc remelting (VAR) process that includes solution of the nonlinear heat conductivity equation with the nonlinear boundary conditions which are typical for VAR process. The finite-difference analogue of the model equations was obtained through the finite volume method. To check the efficiency of the simplified model that does not include magnetohydrodynamic phenomena in the liquid metal pool, the comparison has been made of the numerical calculation of the metal pool depth when melting the Russian titanium alloy VT3-1 with the results of radiographical tests. It was established that the model adequately describes the test data for various melting modes (ingot diameter and current strength).

1. Introduction.

Today a lot of attention is given to automation of VAR furnaces and the focus is on development of the arc clearance control flowcharts, feedback controllers, program management systems for furnace electric modes [1]. Together with the aforementioned issues, the development of the VAR automatic control systems requires a reliable theoretical description of the ingot formation process that underlies the automatic control system algorithms. The significance of through and reliable theoretical models of the ingot process formation is determined by the fact that the immediate control of the ingot parameters during solidification of titanium alloy (in particular, the depth of the metal pool, width of the mushy zone, etc.) using the measuring instruments, appears to be a problem so far. Development of the theoretical ideas about formation of titanium alloy ingots is rather important today since there are cases when different ingot-related defects are observed on billets, bars and eventually on critical parts. Such defects include β -flecks [2], zonal segregation [3], tree-like structure [4] and dark/light spots [5] that may be observed in the transverse section under the macro examination of mill products in different titanium alloys. Very often such defects are related to the final remelting stage therefore the theoretical description of the processes that take

place during solidification of the VAR melted ingots, as well as understanding of the impact of various melting parameters on ingot metallurgical quality, is undoubtedly the paramount objective for creation of the fully automated VAR control system.

Many researchers studied the heat processes in ingots during VAR [6, 7, 8], electroslag remelt [8, 9] and continuous casting [10]. Today, in view of development of advanced computers it is getting important to write science-based VAR simulation programs for their use in industrial environment in order to develop new remelting modes for complex titanium alloys.

Taking into account aforementioned facts we reviewed in this article the mathematical model of the vacuum arc remelting and compared the theoretical calculation of the metal pool depth with the radiographical test results obtained for Russian titanium alloy VT3-1 (Ti-6.5Al-2.5Mo-1.5Cr-0.5Fe-0.3Si) [11]. Taking into consideration the non-trivial complexity and essential non-linearity of the task, it should be noted that firstly there is no exact analytical solution of the task and secondly today there are a lot of different methods of approximation of the boundary conditions and building of the difference schemes for the heat conductivity equation. It is obvious that in such situation the experimental check of the computational solutions obtained through different methods of approximation is getting important. Therefore, in this article we reviewed both aspects of the problem: making the mathematical model and comparison of this model with the experimental results.

2. Vacuum arc remelting process.

We will describe the heat flows during the vacuum arc remelting through the heat conductivity equation that includes release of latent heat within the interval of the alloy solidification. In order not to involve the complex interface conditions on the phase boundary, we reviewed the so-called method of apparent heat capacity [10] that allows to include crystallization rate (i.e. heat source) into the system heat capacity as a complementary additive term [9]. Such problem statement allows to make calculation in one domain without "distinguishing" the liquid, solid and mushy zone.

Also, from this point on we considered that density, heat capacity, heat conductivity and heat-transfer coefficient depend on the temperature in an arbitrary way [12].

Heat transfer equation for VAR ingot can be written in a form

$$\rho(T)C(T)\frac{\partial T}{\partial \tau} = \frac{1}{r}\frac{\partial}{\partial r}\left(r\lambda(T)\frac{\partial T}{\partial r}\right) + \frac{\partial}{\partial z}\left(\lambda(T)\frac{\partial T}{\partial z}\right), \quad (1)$$

where T is temperature, τ is time, $C(T)$ is heat capacity, $\lambda(T)$ is heat conductivity, $\rho(T)$ is density, r and z are radial and axial coordinates.

The boundary may be divided into several areas shown in Figure 1. Such division is based on physical processes that take place on the ingot surface under VAR. We will consider those processes and the relevant boundary conditions.

Boundary AB. On the ingot axis we have the simple symmetry condition:

$$\frac{\partial T}{\partial r} = 0. \quad (2)$$

Boundary BC. The border BC corresponds to a bath mirror surface which are being under an end face of the consumable electrode. On this border we shall set temperature. In the elementary kind the temperature of a surface of a bath is defined by an overheat above alloy liquidus temperature [6]:

$$T = T_L + \Delta T, \quad (3)$$

where T_L is liquidus temperature, ΔT is overheat.

Boundary CD. The boundary CD corresponds to a ring gap. Here we also set a boundary condition of the I-st kind

$$T = T_L + \frac{D_{cr} - 2r}{D_{cr} - D_{el}} \cdot \Delta T, \quad (4)$$

where D_{cr} is crucible diameter, D_{el} is electrode diameter.

Boundary DE. The given boundary corresponds to a zone of a contact belt for which experimental values of a specific thermal flux q [13] are known, therefore we write down a boundary condition of II-nd kind

$$-\lambda(T) \frac{\partial T}{\partial r} = q. \quad (5)$$

Boundary EF. The site EF corresponds to a zone of forming ingot on which has already partially or completely occurred separation of solid ingot from a crucible surface due to passage of process volumetric shrinkage.

Thus three possible mechanisms of heat removal can be observed:

- Heat removal by radiation through the formed gap.
- Heat removal by contact way in places of contact of a surface of an ingot with an internal wall of copper crucible.
- The heat transfer by convection through a gas phase in a gap.

Three specified mechanisms, it is possible to write down the boundary condition considering all in the form of

$$-\lambda(T) \frac{\partial T}{\partial r} = \eta \left(\epsilon \sigma_0 (T^4 - T_{cr}^4) + \frac{k}{d} (T - T_{cr}) \right) + (1 - \eta) \alpha (T - T_{cr}), \quad (6)$$

where η – factor describing a share of contact of a surface of an ingot with a crucible, ϵ – emissivity, T_{cr} is temperature of inner surface of the crucible, α is heat transfer

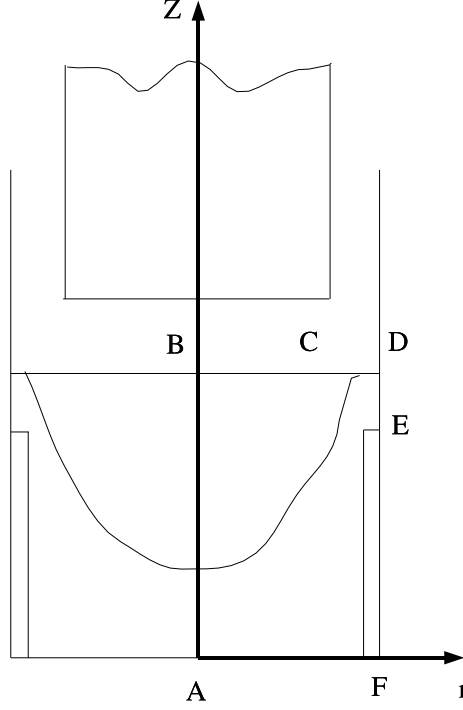


Figure 1. Vacuum arc remelting process.

coefficient in the contact zone, k is heat conductivity of gas in gap, d is gap. The parameters η , ϵ , T_{cr} , α , k , d are depending on temperature. For simplification of a record we shall indicate a following designation

$$\beta_{cr}(T) = \eta_{cr} \left(\epsilon \sigma_0 \frac{T^4 - T_{cr}^4}{T - T_{cr}} + \frac{k}{d} \right) + (1 - \eta_{cr}) \alpha_{cr}, \quad (7)$$

and (6) is rewritten in a more compact form

$$-\lambda(T) \frac{\partial T}{\partial r} = \beta_{cr}(T) (T - T_{cr}). \quad (8)$$

Thus, complex process of the heat transfer on border EF is described with the *nonlinear* law (8).

Boundary FA. On a site FA boundary condition is similar to (8), therefore we shall write down:

$$-\lambda(T) \frac{\partial T}{\partial r} = \beta_{bot}(T) (T - T_{bot}), \quad (9)$$

where

$$\beta_{bot}(T) = \eta_{bot} \left(\epsilon \sigma_0 \frac{T^4 - T_{bot}^4}{T - T_{bot}} + \frac{k}{d} \right) + (1 - \eta_{bot}) \alpha_{bot}. \quad (10)$$

Besides it is necessary for us to set the initial condition for the equation (1). During vacuum arc remelting melt an ingot occurs, i.e. the border BCD moves upwards with the speed defined by remelting conditions. Melting rate of an ingot is defined by the mass speed of fusion depending on force of a current, an electrode and a filled crystallizer diameters, and also on some other parameters. We shall accept in the beginning of remelting is already available ingot of some small height with homogeneous distribution of temperature on all volume is considered to be as the initial condition. Initial temperature it is accepted equal $T_L + \Delta T$. For the subsequent moments of time the initial condition is defined by distribution of temperature during the previous moment of time with additional small layer of an ingot which temperature is $T_L + \Delta T$.

In the following sections we shall consider discretization of the given problem on a rectangular grid, including linearization of a system, and decision method of the received the linear equations system.

3. Discretization of heat conduction equation.

We will consider the most common case when $\lambda(T)$ and $\rho(T)C(T)$ are piecewise continuous functions. In this case it is convenient to use the integral identity method to the finite-difference scheme construct [12]. We introduce the heat fluxes along r and z directions:

$$Q(r, z) = \lambda(r, z) \frac{\partial T}{\partial r}, \quad (11)$$

$$P(r, z) = \lambda(r, z) \frac{\partial T}{\partial z}. \quad (12)$$

Taking into account these notations, Eq. (1) is rewrited to

$$\rho(T)C(T) \frac{\partial T}{\partial \tau} = \frac{1}{r} \frac{\partial}{\partial r} (rQ(r, z)) + \frac{\partial}{\partial z} (P(r, z)). \quad (13)$$

Integrating the Eq. (13) over the cylindric volume for $r \in [r_{i-1/2}, r_{i+1/2}]$ and $z \in [z_{j-1/2}, z_{j+1/2}]$ (see Figure 2) we can write heat balance equation can be put as follows

$$\begin{aligned} & \int_{r_{i+1/2}}^{r_{i-1/2}} r dr \int_{z_{j+1/2}}^{z_{j-1/2}} dz \rho(r, z) C(r, z) \frac{\partial T(r, z)}{\partial \tau} \\ &= \int_{z_{j-1/2}}^{z_{j+1/2}} \left[r_{i+1/2} Q(r_{i+1/2}, z) - r_{i-1/2} Q(r_{i-1/2}, z) \right] dz \\ &+ \int_{r_{i-1/2}}^{r_{i+1/2}} \left[P(r, z_{j+1/2}) - P(r, z_{j-1/2}) \right] r dr. \end{aligned} \quad (14)$$

This equation is *exact*. Now we need to evaluate the integrals, which contains Eq. (14). Because we have (11) than

$$\int_{r_i}^{r_{i+1}} \frac{Q(r, z)}{\lambda(r, z)} dr = T(r_{i+1}) - T(r_i). \quad (15)$$

On the other hand

$$\int_{r_i}^{r_{i+1}} \frac{Q(r, z)}{\lambda(r, z)} dr \approx Q(r_{i+1/2}, z) \int_{r_i}^{r_{i+1}} \frac{dr}{\lambda(r, z)}. \quad (16)$$

Thus we can write following expressions within the fluxes for internal region of ingot

$$Q(r_{i+1/2}, z) \approx \frac{T(r_{i+1}, z) - T(r_i, z)}{\int_{r_i}^{r_{i+1}} \frac{dr}{\lambda(r, z)}}, \quad (17)$$

$$Q(r_{i-1/2}, z) \approx \frac{T(r_i, z) - T(r_{i-1}, z)}{\int_{r_{i-1}}^{r_i} \frac{dr}{\lambda(r, z)}}, \quad (18)$$

$$P(r, z_{j+1/2}) \approx \frac{T(r, z_{j+1}) - T(r, z_j)}{\int_{z_j}^{z_{j+1}} \frac{dz}{\lambda(r, z)}}, \quad (19)$$

$$P(r, z_{j-1/2}) \approx \frac{T(r, z_j) - T(r, z_{j-1})}{\int_{z_{j-1}}^{z_j} \frac{dz}{\lambda(r, z)}}. \quad (20)$$

Let these expressions be substituted in Eq. (14) then

$$\begin{aligned} & \int_{r_{i+1/2}}^{r_{i-1/2}} r dr \int_{z_{j+1/2}}^{z_{j-1/2}} dz \rho(r, z) C(r, z) \frac{\partial T(r, z)}{\partial \tau} \\ &= r_{i+1/2} [T_{i+1,j} - T_{i,j}] \int_{z_{j-1/2}}^{z_{j+1/2}} \frac{dz}{\int_{r_i}^{r_{i+1}} \frac{dr}{\lambda(r, z)}} - r_{i-1/2} [T_{i,j} - T_{i-1,j}] \int_{z_{j-1/2}}^{z_{j+1/2}} \frac{dz}{\int_{r_{i-1}}^{r_i} \frac{dr}{\lambda(r, z)}} \\ &+ [T_{i,j+1} - T_{i,j}] \int_{r_{i-1/2}}^{r_{i+1/2}} \frac{r dr}{\int_{z_j}^{z_{j+1}} \frac{dz}{\lambda(r, z)}} + [T_{i,j} - T_{i,j-1}] \int_{r_{i-1/2}}^{r_{i+1/2}} \frac{r dr}{\int_{z_{j-1}}^{z_j} \frac{dz}{\lambda(r, z)}}. \end{aligned} \quad (21)$$

Making use the simplest approximation for the integral in the left side of equation we obtain

$$\begin{aligned}
& \left(z_{j-1/2} - z_{j+1/2} \right) \frac{r_{i+1/2}^2 - r_{i-1/2}^2}{2} \rho_{i,j} C_{i,j} \frac{\hat{T}_{i,j} - T_{i,j}}{\tau} \\
&= r_{i+1/2} [T_{i+1,j} - T_{i,j}] \int_{z_{j-1/2}}^{z_{j+1/2}} \frac{dz}{\int_{r_i}^{r_{i+1}} \frac{dr}{\lambda(r,z)}} - r_{i-1/2} [T_{i,j} - T_{i-1,j}] \int_{z_{j-1/2}}^{z_{j+1/2}} \frac{dz}{\int_{r_{i-1}}^{r_i} \frac{dr}{\lambda(r,z)}} \\
&+ [T_{i,j+1} - T_{i,j}] \int_{r_{i-1/2}}^{r_{i+1/2}} \frac{rdr}{\int_{z_j}^{z_{j+1}} \frac{dz}{\lambda(r,z)}} + [T_{i,j} - T_{i,j-1}] \int_{r_{i-1/2}}^{r_{i+1/2}} \frac{rdr}{\int_{z_{j-1}}^{z_j} \frac{dz}{\lambda(r,z)}}. \tag{22}
\end{aligned}$$

Moreover the integrals containing heat conductivity is simplified up to:

$$\begin{aligned}
& \int_{z_{j-1/2}}^{z_{j+1/2}} \frac{dz}{\int_{r_i}^{r_{i+1}} \frac{dr}{\lambda(r,z)}} \approx \frac{z_{j+1/2} - z_{j-1/2}}{r_{i+1} - r_i} \cdot \lambda_{i+1/2,j}, \\
& \int_{z_{j-1/2}}^{z_{j+1/2}} \frac{dz}{\int_{r_{i-1}}^{r_i} \frac{dr}{\lambda(r,z)}} \approx \frac{z_{j+1/2} - z_{j-1/2}}{r_i - r_{i-1}} \cdot \lambda_{i-1/2,j}, \\
& \int_{r_{i-1/2}}^{r_{i+1/2}} \frac{rdr}{\int_{z_j}^{z_{j+1}} \frac{dz}{\lambda(r,z)}} \approx \frac{r_{i+1/2}^2 - r_{i-1/2}^2}{2(z_{j+1} - z_j)} \cdot \lambda_{i,j+1/2}, \\
& \int_{r_{i-1/2}}^{r_{i+1/2}} \frac{rdr}{\int_{z_{j-1}}^{z_j} \frac{dz}{\lambda(r,z)}} \approx \frac{r_{i+1/2}^2 - r_{i-1/2}^2}{2(z_j - z_{j-1})} \cdot \lambda_{i,j-1/2}.
\end{aligned}$$

After that the Eq. (22) can be rewritten as

$$\begin{aligned}
& \rho_{i,j} C_{i,j} \frac{\hat{T}_{i,j} - T_{i,j}}{\tau} = \\
& (T_{i+1,j} - T_{i,j}) \cdot \lambda_{i+1/2,j} \cdot \frac{r_{i+1/2}}{r_{i+1} - r_i} \cdot \frac{2}{r_{i+1/2}^2 - r_{i-1/2}^2} \\
& - (T_{i,j} - T_{i-1,j}) \cdot \lambda_{i-1/2,j} \cdot \frac{r_{i-1/2}}{r_i - r_{i-1}} \cdot \frac{2}{r_{i+1/2}^2 - r_{i-1/2}^2} \\
& + (T_{i,j+1} - T_{i,j}) \cdot \lambda_{i,j+1/2} \cdot \frac{1}{(z_{j+1} - z_j) \cdot (z_{j+1/2} - z_{j-1/2})} \\
& - (T_{i,j} - T_{i,j-1}) \cdot \lambda_{i,j-1/2} \cdot \frac{1}{(z_j - z_{j-1}) \cdot (z_{j+1/2} - z_{j-1/2})}. \tag{23}
\end{aligned}$$

We define (for the simplest way)

$$r_{i+1/2} = \frac{r_i + r_{i+1}}{2}, \quad r_{i-1/2} = \frac{r_{i-1} + r_i}{2},$$

$$z_{j+1/2} = \frac{z_j + z_{j+1}}{2}, \quad z_{j-1/2} = \frac{z_{j-1} + z_j}{2}.$$

Thus for the rectangular grid Eq. (23) can be written in the common form as

$$\begin{aligned} \rho_{i,j} C_{i,j} \frac{\hat{T}_{i,j} - T_{i,j}}{\tau} &= \frac{r_{i+1} + r_i}{r_{i+1} - r_i} \cdot \frac{4\lambda_{i+1/2,j}}{(r_{i+1} + r_i)^2 - (r_i - r_{i-1})^2} \cdot [T_{i+1,j} - T_{i,j}] \\ &- \frac{r_i + r_{i-1}}{r_i - r_{i-1}} \cdot \frac{4\lambda_{i-1/2,j}}{(r_{i+1} + r_i)^2 - (r_i - r_{i-1})^2} \cdot [T_{i,j} - T_{i-1,j}] \\ &+ \frac{2\lambda_{i,j+1/2}}{(z_{j+1} - z_j) \cdot (z_{j+1} - z_{j-1})} \cdot [T_{i,j+1} - T_{i,j}] \\ &- \frac{2\lambda_{i,j-1/2}}{(z_j - z_{j-1}) \cdot (z_{j+1} - z_{j-1})} \cdot [T_{i,j} - T_{i,j-1}]. \end{aligned} \quad (24)$$

For constant space steps (h_r and h_z) we have

$$\begin{aligned} \rho_{i,j} C_{i,j} \frac{\hat{T}_{i,j} - T_{i,j}}{\tau} &= \frac{\lambda_{i+1/2,j}}{h_r^2} \cdot \left(1 + \frac{1}{2i}\right) [T_{i+1,j} - T_{i,j}] - \frac{\lambda_{i-1/2,j}}{h_r^2} \cdot \left(1 - \frac{1}{2i}\right) [T_{i,j} - T_{i-1,j}] + \\ &+ \frac{\lambda_{i,j+1/2}}{h_z^2} \cdot [T_{i,j+1} - T_{i,j}] - \frac{\lambda_{i,j-1/2}}{h_z^2} \cdot [T_{i,j} - T_{i,j-1}]. \end{aligned} \quad (25)$$

To evaluate heat conductivity at the semi - integer domain points we use approximation [14]

$$\begin{aligned} \lambda_{i+1/2,j} &= \frac{2\lambda_{i,j}\lambda_{i+1,j}}{\lambda_{i,j} + \lambda_{i+1,j}}, & \lambda_{i-1/2,j} &= \frac{2\lambda_{i-1,j}\lambda_{i,j}}{\lambda_{i-1,j} + \lambda_{i,j}}, \\ \lambda_{i,j+1/2} &= \frac{2\lambda_{i,j}\lambda_{i,j+1}}{\lambda_{i,j} + \lambda_{i,j+1}}, & \lambda_{i,j-1/2} &= \frac{2\lambda_{i,j-1}\lambda_{i,j}}{\lambda_{i,j} + \lambda_{i,j-1}}. \end{aligned} \quad (26)$$

Equation (25) joins the temperature $T_{i,j}$ with $T_{i-1,j}$, $T_{i+1,j}$, $T_{i,j-1}$ and $T_{i,j+1}$, than Eq. (25) has 5-point space scheme and explicit scheme in time. We will use 2-cycle scheme [12]. Let we rewrite Eq. (25) as follows

$$\rho_{i,j} C_{i,j} \frac{\hat{T}_{i,j} - T_{i,j}}{\tau} = \Lambda_r T_{i,j} + \Lambda_z T_{i,j}, \quad (27)$$

where operators $\Lambda_{r,z}$ are defined by Eq. (25). The main idea of the 2-cycle factorization scheme is making of the following steps (k is time step index) [12]

$$\rho_{i,j} C_{i,j} \frac{T_{i,j}^{k-1/2} - T_{i,j}^{k-1}}{\tau} = \Lambda_r \frac{T_{i,j}^{k-1/2} + T_{i,j}^{k-1}}{2} \quad (28)$$

$$\rho_{i,j} C_{i,j} \frac{T_{i,j}^k - T_{i,j}^{k-1/2}}{\tau} = \Lambda_z \frac{T_{i,j}^k + T_{i,j}^{k-1/2}}{2} \quad (29)$$

$$\rho_{i,j} C_{i,j} \frac{T_{i,j}^{k+1/2} - T_{i,j}^k}{\tau} = \Lambda_z \frac{T_{i,j}^{k+1/2} + T_{i,j}^k}{2} \quad (30)$$

$$\rho_{i,j} C_{i,j} \frac{T_{i,j}^{k+1} - T_{i,j}^{k+1/2}}{\tau} = \Lambda_r \frac{T_{i,j}^{k+1} + T_{i,j}^{k+1/2}}{2} \quad (31)$$

The cycle of evaluation is namely to solve equations (28)-(31). Let we rewrite these equations in a more useful form

$$\begin{aligned} [B_{i,j}] T_{i-1,j}^{k-1/2} - [A_{i,j} + B_{i,j} + 2\rho_{i,j} C_{i,j}/\tau] T_{i,j}^{k-1/2} + [A_{i,j}] T_{i+1,j}^{k-1/2} \\ = - \left([B_{i,j}] T_{i-1,j}^{k-1} - [A_{i,j} + B_{i,j} - 2\rho_{i,j} C_{i,j}/\tau] T_{i,j}^{k-1} + [A_{i,j}] T_{i+1,j}^{k-1} \right) \end{aligned} \quad (32)$$

$$\begin{aligned} [\Delta_{i,j}] T_{i,j-1}^k - [\Delta_{i,j} + \Gamma_{i,j} + 2\rho_{i,j} C_{i,j}/\tau] T_{i,j}^k + [\Gamma_{i,j}] T_{i,j+1}^k \\ = - \left([\Delta_{i,j}] T_{i,j-1}^{k-1/2} - [\Delta_{i,j} + \Gamma_{i,j} - 2\rho_{i,j} C_{i,j}/\tau] T_{i,j}^{k-1/2} + [\Gamma_{i,j}] T_{i,j+1}^{k-1/2} \right) \end{aligned} \quad (33)$$

$$\begin{aligned} [B_{i,j}] T_{i-1,j}^{k+1/2} - [A_{i,j} + B_{i,j} + 2\rho_{i,j} C_{i,j}/\tau] T_{i,j}^{k+1/2} + [A_{i,j}] T_{i+1,j}^{k+1/2} \\ = - \left([B_{i,j}] T_{i-1,j}^k - [A_{i,j} + B_{i,j} - 2\rho_{i,j} C_{i,j}/\tau] T_{i,j}^k + [A_{i,j}] T_{i+1,j}^k \right) \end{aligned} \quad (34)$$

$$\begin{aligned} [\Delta_{i,j}] T_{i,j-1}^{k+1} - [\Delta_{i,j} + \Gamma_{i,j} + 2\rho_{i,j} C_{i,j}/\tau] T_{i,j}^{k+1} + [\Gamma_{i,j}] T_{i,j+1}^{k+1} \\ = - \left([\Delta_{i,j}] T_{i,j-1}^{k+1/2} - [\Delta_{i,j} + \Gamma_{i,j} - 2\rho_{i,j} C_{i,j}/\tau] T_{i,j}^{k+1/2} + [\Gamma_{i,j}] T_{i,j+1}^{k+1/2} \right) \end{aligned} \quad (35)$$

where we denoted

$$B_{i,j} = \frac{\lambda_{i-1/2,j}}{h_r^2} \left(1 - \frac{1}{2i} \right), \quad A_{i,j} = \frac{\lambda_{i+1/2,j}}{h_r^2} \left(1 + \frac{1}{2i} \right). \quad (36)$$

$$\Delta_{i,j} = \frac{\lambda_{i,j-1/2}}{h_z^2}, \quad \Gamma_{i,j} = \frac{\lambda_{i,j+1/2}}{h_z^2}. \quad (37)$$

The solving of these equations is strightforward, because equation matrixes are three-diagonal, then these equations have 3-point space scheme. It is a very important note for our method, because we will have possibility to decrease CPU time.

It might to prove 2-cycle method is absolutly time step stability [12] and it has second-order in τ^2 like Crank-Nicholson scheme and second-order in space. Moreover defferential operators $\Lambda_{r,z}$ in the 2-cycle method can be noncommutating ones.

4. Discretization of boundary conditions.

To solve the equations (32)-(35) it is necessary to define values of temperature on border or to set some relationships connecting temperature on border of a body with temperature of an environment. Boundary conditions in a continuous limit are certain by equations (2) - (9). We shall construct their discrete finite difference analogues on the uniform grid, using a method of finite volume [14]. For this purpose we shall integrate the equation (13) on some volume G , adjoining to border of an ingot and on time within the limits of $[t, t + \tau]$. Such volumes are shown on Fig. 2.

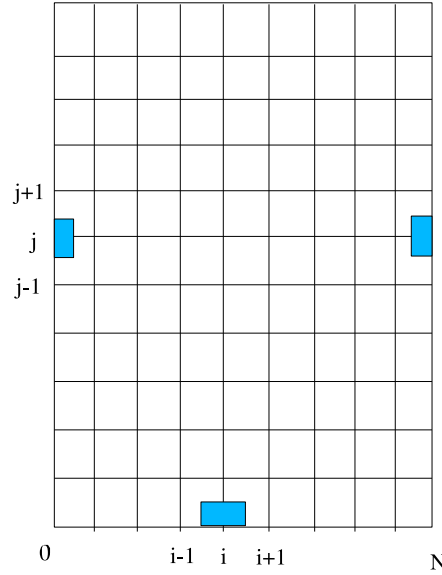


Figure 2. The volumes for evaluating of integral balances in the boundary conditions.

Integral balance of heat can be written as

$$\int_t^{t+\tau} \int_G \rho(T)C(T) \frac{\partial T}{\partial t} dV dt = \int_t^{t+\tau} \int_G \left(\frac{1}{r} \frac{\partial}{\partial r} (rQ) + \frac{\partial P}{\partial z} \right) dV dt, \quad (38)$$

where heat fluxes are defined by Eqs. (11) and (12).

After integration we shall receive the relationship connecting a thermal flux on border of a body, set by a corresponding boundary condition, and thermal fluxes in nearby points for which some approximations are required. Integration on time is led as follows: the left part of the Eq. (38) we approximate as follows

$$\int_t^{t+\tau} \int_G \rho(T)C(T) \frac{\partial T}{\partial t} dV dt \sim \hat{T} - T, \quad (39)$$

and the right part of Eq. (38) we shall calculate in *previous* the moment of time. Now it is easy to calculate finite difference counterparts of boundary conditions.

4.1. Boundary AB.

Let area $G = [0, h_r/2] \times [(j - 1/2)h_z, (j + 1/2)h_z]$ then the general expression for a boundary condition on a site AB after integration can be written down in the form of

$$\begin{aligned} \frac{h_r^2 h_z}{8} \rho C_{0,j} [\hat{T}_{0,j} - T_{0,j}] &= \frac{\tau h_z}{2} \lambda_{1/2,j} [T_{1,j} - T_{0,j}] \\ &+ \frac{\tau h_r^2}{8 h_z} \left(\lambda_{0,j+1/2} [T_{0,j+1} - T_{0,j}] - \lambda_{0,j-1/2} [T_{0,j} - T_{0,j-1}] \right). \end{aligned} \quad (40)$$

4.2. Boundary BC.

On a site BC there is no necessity to use a method of finite volume as in this case the field of temperatures is set directly, therefore

$$\hat{T}_{i,M} = T_L + \Delta T. \quad (41)$$

4.3. Boundary CD.

On a site CD we set the temperature, as well as on BC

$$\hat{T}_{i,M} = T_L + \frac{D_{cr} - 2ih_r}{D_{cr} - D_{el}} \Delta T. \quad (42)$$

4.4. Boundary DE.

Let $G = [(N - 1)h_r, Nh_r] \times [(j - 1/2)h_z, (j + 1/2)h_z]$ then the general expression for a boundary condition on a site DE after integration it is possible to write down in the form of

$$\begin{aligned} \frac{h_r^2 h_z}{8} (4N - 1) \rho C_{N,j} [\hat{T}_{N,j} - T_{N,j}] &= -\tau h_z N h_r q - \tau h_z \left(N - \frac{1}{2}\right) \lambda_{N-1/2,j} [T_{N,j} - T_{N-1,j}] \\ &+ \frac{\tau h_r^2}{8 h_z} (4N - 1) \left(\lambda_{N,j+1/2} [T_{N,j+1} - T_{N,j}] - \lambda_{N,j-1/2} [T_{N,j} - T_{N,j-1}] \right). \end{aligned} \quad (43)$$

4.5. Boundary EF.

Let $G = [(N - 1)h_r, Nh_r] \times [(j - 1/2)h_z, (j + 1/2)h_z]$ then the general expression for a boundary condition on a site EF after integration it is possible to write down area in the form of

$$\begin{aligned}
& \frac{h_r^2 h_z}{8} (4N - 1) \rho C_{N,j} [\hat{T}_{N,j} - T_{N,j}] \\
& = -\tau h_z N h_r \beta_{N,j}^{cr} [T_{N,j} - T_{cr}] + \tau h_z (N - \frac{1}{2}) \lambda_{N-1/2,j} [T_{N,j} - T_{N-1,j}] \\
& + \frac{\tau h_r^2}{8 h_z} (4N - 1) \left(\lambda_{N,j+1/2} [T_{N,j+1} - T_{N,j}] - \lambda_{N,j-1/2} [T_{N,j} - T_{N,j-1}] \right) \quad (44)
\end{aligned}$$

4.6. Boundary AF.

Let $G = [(i - 1/2)h_r, (i + 1/2)h_r] \times [0, h_z/2]$ then the general expression for a boundary condition on a site FA after integration it is possible to write down area in the form of

$$\begin{aligned}
& \frac{i h_r^2 h_z}{2} \rho C_{i,0} [\hat{T}_{i,0} - T_{i,0}] \\
& = \frac{i \tau h_r^2}{h_z} \left(\lambda_{i,1/2} [T_{i,1} - T_{i,0}] - h_z \beta_{i,0} [T_{i,0} - T] \right) \\
& = \tau h_z \left(\left(i + \frac{1}{2} \right) \lambda_{i+1/2,0} [T_{i+1,0} - T_{i,0}] - \left(i - \frac{1}{2} \right) \lambda_{i-1/2,0} [T_{i,0} - T_{i-1,0}] \right) \quad (45)
\end{aligned}$$

Further we use approximations for heat conductivity factors in semi-integer points, similar to Eq. (26)

5. The model parameters for VT3-1 alloy.

As it is possible to see from expressions for boundary conditions on a mirror of a liquid bath (BC and CD) we set distribution of temperature which is defined by alloy liquidus temperature and an overheat depending on parameters of VAR. The overheat of the melt Δ can be described by formula [3]:

$$\Delta T(J, D_{in}) = 400 e^{-12 \frac{D_{in}}{J}}, \quad (46)$$

where J is arc current, kA; D_{in} – ingot diameter, m. In a zone DE the thermal flux q to which measurements for alloy VT3-1 work [13] is devoted is set. The parameter η defines the relative contribution of each of mechanisms of heat removal: at $\eta = 1$ the heat-conducting path goes only by radiation, and at $\eta = 0$ only by convection. For EF we accepted $\eta_{EF} = 1.0$, and for FA – $\eta_{FA} = 0.5$.

$C(T)$, including rate of release of latent heat in an interval of temperatures between liquidus T_L and solidus T_S , it is possible to present an effective specific thermal capacity in the form of [10]:

$$C(T) = \begin{cases} C_L(T) & \text{for } T > T_L \\ g(T)C_S(T) + [1 - g(T)]C_L(T) - L \frac{dg(T)}{dT} & \text{for } T_S \leq T \leq T_L \\ C_S(T) & \text{for } T < T_S \end{cases} \quad (47)$$

where C_L and C_S are specific heat capacities for liquid and solid phases; L is latent heat of fusion, $g(T)$ is solid fraction. In case of binary alloy for $g(T)$ we can obtain simple expression (under lever rule suggestion)

$$g(T) = \frac{T_m - T_S}{T_L - T_S} \cdot \frac{T_L - T}{T_m - T}. \quad (48)$$

For temperature derivative of $g(T)$ we can obtain

$$\frac{dg(T)}{dT} = -\frac{T_m - T_L}{T_L - T_S} \cdot \frac{T_m - T_S}{(T_m - T)^2}, \quad (49)$$

where T_m is fusion temperature of a solvent, T_L is liquidus temperature, T_S is solidus temperature. Parameters of model for alloy VT3-1 have been chosen by the following $T_m = 1668 \text{ }^\circ\text{C}$, $T_S = 1550 \text{ }^\circ\text{C}$, $T_L = 1620 \text{ }^\circ\text{C}$, $L = 355000 \text{ J/kg}$, $T_{cr} = 70 \text{ }^\circ\text{C}$, $T_{bot} = 70 \text{ }^\circ\text{C}$, $\alpha_{bot} = 300 \text{ W/m}^2 \text{ K}$. Some data can be found in [15]. Position of a point E was defined as in work [6].

For the account of increase in heat conductivity due to fluid flow we have increased heat conductivity of an alloy in a liquid phase [6]. Temperature dependence of the resulted ingot surface emissivity degree and an internal surface of crucible has been chosen in the form of square-law dependence on temperature [15].

6. Simulation results and radiographical experiments.

Using the mathematical model described above, we have led solidification modelling of ingots from the alloy VT3-1. Modes of remeltings are specified in the Table 1.

Some works [3, 11] describe the experimental research of the metal pool depth and profile through fixation with radioactive isotopes. Below we compare the simulation results with the experimental data on liquid metal pool depth at different points of time. In order to adequately describe the experimental data we have carried out "adjusting" of the model. The adjusting provided for rather exact match of the calculated and experimental metal pool depth, as well as liquid metal pool profiles at different ingot height. Due to the fact that the most extensive experimental data are available for 750 mm dia ingot melted at 37 kA, we carried out "adjusting" for the above-mentioned melting mode. The main variable parameters were – heat conductivity in the liquid phase (that was considered not dependent on temperature) and the surface emissivity factor depending on temperature.

Table 1. Remelting regimes.

Ingot diameter, mm	Arc current, kA
750	37
570	25
435	15

6.1. $\phi 750$ mm ingot. Arc current $J = 37$ kA.

One of the most important parameters assessed during analysis of one or another VAR mode for titanium alloys (as well as for nickel-base, iron-base and zirconium base alloys [6, 7, 8, 10]) is the depth of the liquid metal pool. Figure 3 shows the theoretical metal pool depth with experimentally obtained depth (through fixation with tungsten radioactive isotopes) depending on the height of the melted ingot. As is obviously, the theory describes the metal pool depth behavior satisfactorily. During melting the quasi-steady state was achieved at the metal pool depth having been steady.

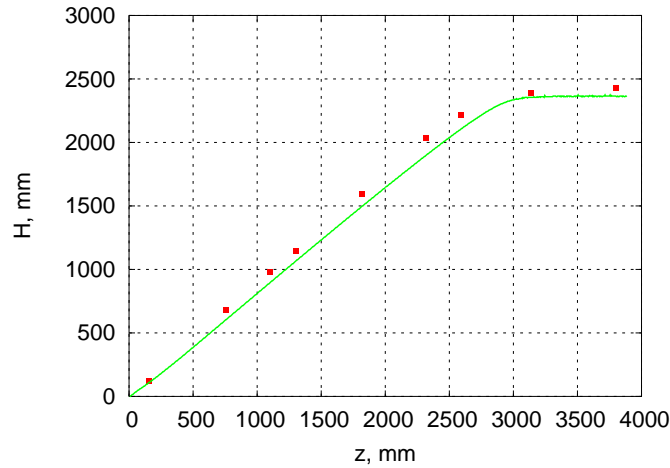


Figure 3. Experimental and theoretical pool depth versus the height of the melted ingot. $\phi 750$ mm ingot, arc current $J = 37$ kA. Points – experiment, curve – theory.

The description of the liquid metal pool only *may be misleading* as the pool depth does not actually reflect the volume of the liquid metal at the particular melt point. In order to assess feasibility of satisfactory simulation of the liquid metal pool volume using the model, we calculated the liquid metal pool profiles at the points of time recorded on the experimental radiogram. This shows that the model adequately simulates the profiles of the liquid metal pool during the whole melt process. All this together suggests that on the basis of the simulation approach in question it is feasible to simulate some most important parameters of metal solidification under VAR (width of mushy zone, temperature gradient, isotherm travel rate).

Figure 4 shows the calculated profiles of the liquid metal pool during first 140 minutes of melting (with 20 minute interval) to evaluate the linear solid-melt interface travel rate in different ingot zones. The comparison of the simulated profiles with the experimentally obtained metal pool profiles shows that the simulated metal pool volumes do not deviate from the experimental ones by more than 15%.

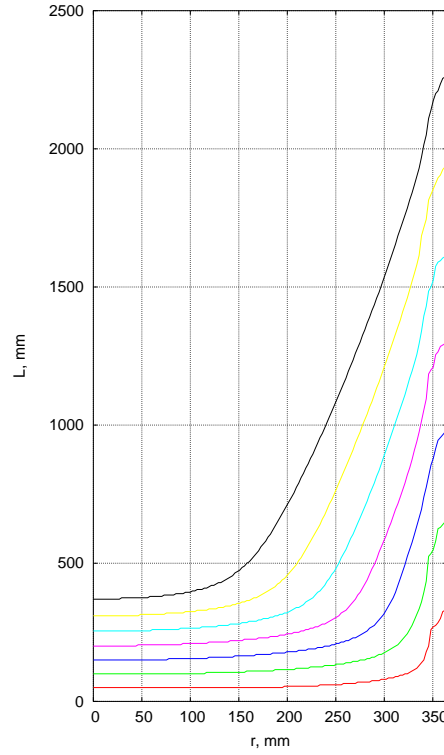


Figure 4. Calculated profiles of the liquid metal pool during first 140 minutes of melting (with 20 minute interval).

6.2. $\phi 570$ mm ingot. Arc current $J = 25$ kA.

Figure 5 shows the theoretical curves and experimental points for 570 mm ingot melted at 25 kA. In this case we compared the simulated data with the experimental data according to location of the pool open surface (i.e. melt mirror) and pool bottom coordinate versus the melting time. It can be seen from Figure 5 that the quasi-steady state was not achieved.

6.3. $\phi 435$ mm ingot. Arc current $J = 15$ kA.

Figure 6 shows the theoretical curves and experimental points for 435 mm ingot melted at 15 kA. In this case as above we compared the simulated data with the experimental data according to location of the pool open surface (i.e. melt mirror) and pool bottom coordinate versus the melting time. It can be seen from Figure 6 that the quasi-steady state was achieved.

Therefore, a conclusion can be made that under *selected* parameters for Vt3-1 alloy, the simulation model can describe the main behavior tendencies of such VAR parameters as liquid metal pool depth and profile at different melting points. It is very important to note that the model that was "adjusted" once, gives satisfactory description of the experimental data beyond the "adjusting values".

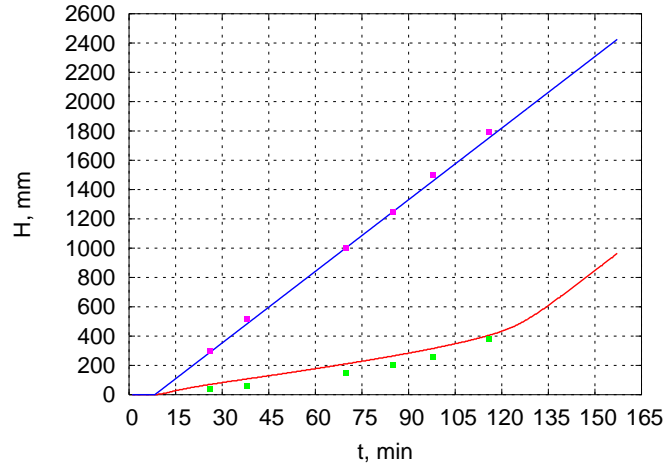


Figure 5. Location of the pool open surface (upper curve and points) and pool bottom coordinate versus the melting time. $\phi 570$ mm ingot, arc current $J = 25$ kA. Theory – curves, experiment – points.

7. Conclusion.

This article describes the mathematical simulation model of heat processes that take place under VAR. The discretization has been made of the *non-linear* heat conductivity equation through the Marchuck's method of integral identities and of *non-linear* boundary conditions through the final volume method. The solution algorithm in question has unconditional numerical stability and is applicable for tasks with non-commuting differentiation operators dependent on time.

For the purposes of the simulation model testing we calculated the liquid metal

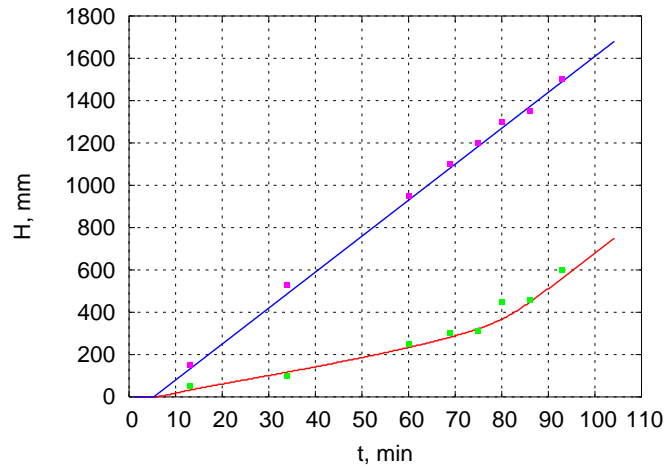


Figure 6. Location of the pool open surface (upper curve and points) and pool bottom coordinate versus the melting time. $\phi 435$ mm ingot, arc current $J = 15$ kA. Theory – curves, experiment – points.

pool depth under VAR melting of titanium alloy VT3-1. It was observed that the model simulates the liquid metal pool (depth and profiles) rather adequately during the whole melting process for different ingot diameters and different current strength. The relative error in determining the liquid metal pool profile does not exceed 15%. This would enable to use the model in future to calculate various melting modes in order to assess such parameters as: liquid metal pool depth, liquid metal pool volume, width of two-phase zone, temperature gradient, isotherms travel rate and local solidification time.

References

- [1] James A. Van Den Avyle, John A. Brooks, and Adam C. Powell. Reducing Defects in Remelting Processes for High-Performance Alloys *JOM*, 50 (3) (1998), pp. 22-25, 49.
- [2] A. Mitchell. Melting, casting and forging problems in titanium alloys *Materials Science and Engineering A243* (1998) 257-262.
- [3] A.L. Andreev, N.F. Anoshkin, G.A. Bochvar et al. Melting and Castings of Titanium Alloys. Metallurgical Press, Moscow, Russian Federation, 1994. (in Russian)
- [4] R.E. Adams, H.W. Rosenberg. Titanium Alloys Solidification *Proceedings Titanium'1974*, Moscow, pp. 85-95.
- [5] E.N. Kondrashov, A.Yu. Maximov, L.V. Konovalov. Dark/bright spots in the Ti-6-4 and Ti-811 alloys. *Laboratory of Titanium Alloys Report 191*, VSMPO, 2005. (in Russian)
- [6] A. Jardy, L. Falk, D. Ablitzer. *Ironmaking and Steelmaking*, 1992, vol.19, 3, pp. 226-232.
- [7] A.F. Wilson, A. Jardy, J. Hamel, S.P. Fox and D. Ablitzer. Implementation and Utilization of a Mathematical Model to Simulate Vacuum Arc Remelting of Titanium Alloys. *Proceedings Titanium'2003*, pp. 149-156.
- [8] L.A. Bertram, P.R. Schunk, S.N. Kempka, F. Spadafora and R. Minisandram. The Macroscale Simulation of Remelting Process. *JOM*, March 1998, pp. 18-21.
- [9] B.I. Medovar, V.L. Shevtsov, G.S. Marinskii, V.F. Demchenko, V.I. Mahnenko. Thermal processes during elctroslag remelting, Kiev, 1978. (in Russian)
- [10] Yu.A. Malevich, Yu.A. Samoilovich. Teplofizicheskie osnovy zatverdevaniya otlivok i slitkov. Minsk, 1989. (in Russian)
- [11] V.V. Tetyukhin, V.N. Kurapov, G.I. Krasheninina et al. Technical report: Investigation of titanium alloys ingots with 150 ~ 770 mm diameters, VSMPO, 1974. (in Russian)
- [12] G.I. Marchuk. Metody vychislitel'noy matematiki. "Nauka", Moscow, 1977, 456 p. (in Russian)
- [13] V.V. Tetyukhin, V.N. Kurapov, Yu.P. Denisov et al. Titanium Alloys Solidification *Proceedings Titanium'1974*, Moscow, pp. 93-97.
- [14] S. Patankar. Numerical heat transfer and fluid flow. New York, "Hemisphere Publishing Corporation", 1980.
- [15] Teplofizicheskie svoystva titana i ego splavov. Eds. A.E. Sheindlin. Moscow, "Metallurgiya", 1985. (in Russian)